Journal of Fluorescence, Vol. 10, No. 3, 2000

Spectroscopic Characterization of Porphyrin-Doped Sol-Gel-Derived Matrices

G. Hungerford,[1] M. I. C. Ferreira,[1,3] M. R. Pereira,[1] J. A. Ferreira,[1] and A. F. Coelho[2]

Received September 28, 1999; revised January 31, 2000; accepted February 1, 2000

Absorption and fluorescence spectra were measured for metal free (HTSPP) and zinc (ZnTSPP) sulfonated porphyrins in SiO_2 and TiO_2 matrices produced by the sol-gel technique. These are compared to correspondent data obtained for the two porphyrins in ethanol at different pH values. In the silica medium (acidic), HTSPP is diprotonated and forms aggregates. This effect is found to be reversed on exposure to ammonia vapor and occurs to a much lower degree in titania matrices. This is possibly because of the smaller amount of solvent retained in the pore structure. The main effect of incorporating ZnTSPP in sol-gel-derived matrices is demetallation, although to a lesser extent than in acidic solution.

KEY WORDS: Sol-gel media; porphyrin; spectroscopy; applications.

INTRODUCTION

Innumerable articles have been published on the spectroscopical and photophysical properties of porphyrins since the pioneering works of Emerson and Rabinowitch [1] and Gouterman [2]. The electronic absorption spectra of these compounds are very distinctive and characterized by the presence of an intense band (the Soret or B band) close to 420 nm, relating to the $S_2 \leftarrow S_0$ transition, and by weaker bands in the region 500 to 650 nm (Q bands), pertaining to the $S_1 \leftarrow S_0$ transition. Among the main quests of porphyrin research are the elucidation of the primary photophysical events of natural photosynthesis in green plants and the search for the optimal *in vitro* photochemical water decomposition systems. This has led to a vast amount of work using porphyrins through studies either in homogeneous solutions or in microheterogeneous media such as vesicles, microemulsions, etc. More recently novel molecular systems, where the porphyrins are incorporated in rigid molecular structures at well-controlled mutual distances, have been shown to be ideal models to study the fundamental mechanisms of electronic energy transfer [3].

Sol-gel-derived synthesis of materials allows the incorporation of organic molecules, thus providing the fabrication of new and versatile materials with applications in many fields such as solid-state lasers, optoelectronics, chemical sensors, etc. [4]. In this way it is possible to study the spectroscopical and photophysical properties of molecules when subject to spatial confinement, for instance, in the structural network of TiO_2 and SiO_2 matrices. Moreover, the expanding field of nonlinear optics has prompted the development of new photonic materials based on the doping of inorganic materials with organic molecules such as porphyrins [5].

In this work we report the steady-state and time-resolved photoluminescence of meso-tetra(4-sulfonatophenyl)porphine and zinc meso-tetra(4-sulfonatophenyl) porphyrin when incorporated in TiO_2 and SiO_2 matrices produced by the sol-gel process. Morphological and struc-

[1] Centro de Física, Instituto de Materiais, Universidade do Minho, 4709-320 Braga, Portugal.
[2] Departamento de Física, Universidade de Trás-os-Montes e Alto Douro, 5001 Vila Real, Portugal.
[3] To whom correspondence should be addressed at Departamento de Física, Universidade do Minho, 4700-320 Braga, Portugal. Fax: +351-253-678981.

1053-0509/00/0900-0283$18.00/0

tural characterization of each matrix was also performed to obtain a better understanding of the porphyrin–host matrix interaction. We have observed that reversible protonation of the porphyrins occurs on incorporation into sol-gel-derived matrices. This was accompanied by strong changes in the optical and spectroscopic properties of these hybrid systems, thus suggesting that they are promising optical sensors for the *in situ* detection of ammonia and acids [6]. Aggregation of porphyrins in general is a well-documented phenomenon [7] and this feature is also present for water-soluble porphyrins in aqueous electrolytes [8]. In our study we have observed that protonation induces aggregation of the porphyrins in ethanolic solutions and in both types of matrices.

EXPERIMENTAL

Sample Preparation

Meso-tetra(4-sulfonatophenyl)porphine dihydrochloride (HTSPP) and zinc meso-tetra(4-sulfonatophenyl)porphyrin dihydrochloride (ZnTSPP) were purchased from Porphyrin Products Inc. and Midcentury, respectively, and used without further purification. Stock solutions of each porphyrin in ethanol were prepared and incorporated during the manufacture of the SiO_2 and TiO_2 matrices by the sol-gel technique. Silica matrices were made from the acid-catalyzed hydrolysis and condensation of tetraethylorthosilicate (TEOS) with ethanol and water, acidified to pH 3 with hydrochloric acid (HCl). After the reaction samples were placed in plastic cuvettes, which were then sealed and placed in an oven at 60°C for more than 2 weeks. TiO_2 matrices were prepared using a mixture of titanium (IV) isoproxide, 2-propanol, ethanol, and deionized water containing HCl. In this case the sealed cuvettes containing transferred reaction mixture were left at room temperature. The seal was broken after a few days and the samples required several weeks before they were considered ready. In both cases this was judged when there was no further apparent decrease in size.

Measurements

The structure of the matrices was examined by X-ray diffractometry (XRD) using a Philips PW1710 diffractometer. Absorption and transmittance spectra were measured on a Shimadzu UV-3101 PC. Steady-state fluorescence measurements were performed using a Spex Fluorolog, while time-resolved measurements were recorded using a single-photon counting spectrometer. This was equipped with a hydrogen-filled coaxial flashlamp excitation source, the required excitation wavelength selected via a monochromator. The fluorescence emission was wavelength selected using a cutoff filter and detection was made using a Hamamatsu R-2949 side window photomultiplier. Cutoff filters were used to obtain a good fluorescence signal necessitated by the use of flashlamp excitation, which also meant that excitation was into the peak absorption band of the samples [usually the Soret (B) band]. Data analysis was performed using software provided by IBH Consultants Ltd. Errors are given as three standard deviations and the proportion of each fluorescing component as a relative amplitude (preexponential factor weighted by the lifetime) to facilitate comparison with the steady-state measurements. All measurements were performed at room temperature.

RESULTS AND DISCUSSION

Characterization of the Matrices

The X-ray diffractograms of both matrices, previously reduced to powder and measured in the high-angle configuration, are shown in Fig. 1. The third diffractogram refers to a natural crystal of anatase [9]. According to this figure the silica matrix is formed as an amorphous silicate hydrate, usually referred to as an opal, whereas the titania diffractogram displays the structural features of the anatase variety of TiO_2 [10]. From detailed analysis of the main diffraction peak ($\theta = 25°$) of titania and according to the treatment proposed by Langford [11], it was possible to obtain the value of 3 nm for the coherence length. This represents the characteristic length of the more structurally ordered domains (anatase) that can be found in the titania matrix.

The void fraction of each matrix and the presence of residual water and ethanol were determined from the experimental values of the refractive index of each undoped sample. Optical transmittance measurement was in the range 400–800 nm and the data were analyzed according to the theory developed by Webman *et al.* [12] for microscopically inhomogeneous disordered materials, when the correlation length is much smaller than the optical wavelength. According to this theory light propagates by multiple scattering in heterogeneous media and so the effective dielectric constant of such media, ε, is related to the dielectric constant of each component, ε_i, by the equation

$$\frac{\varepsilon_i(\omega) - \varepsilon(\omega)}{\varepsilon_i(\omega) + 2\varepsilon(\omega)} = 0 \qquad (1)$$

Assuming each matrix to be a three component system—

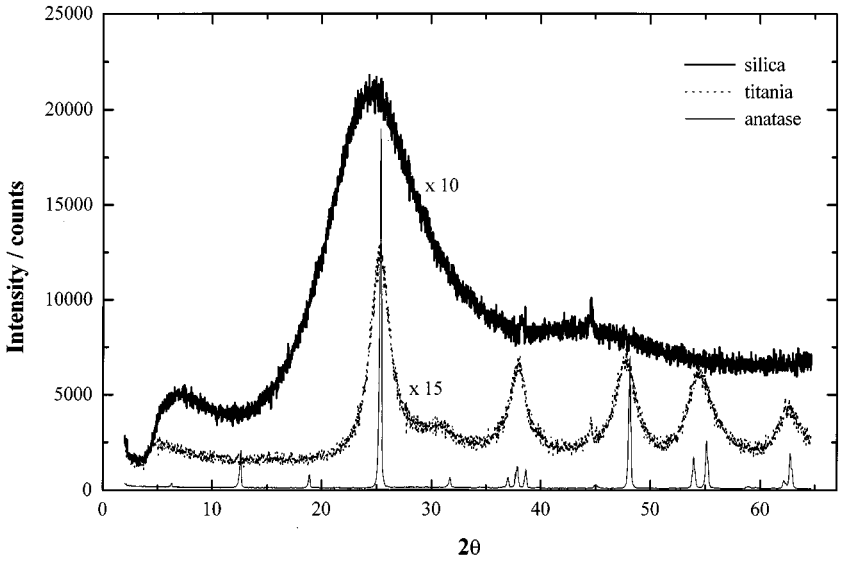

Fig. 1. X-ray diffractograms for both the TEOS and the titanium derived sol-gel matrices. The diffractogram for the anatase form of TiO_2 is also shown for comparison.

medium, solvent mixture, and void—the fractional volume of each component, f_i, can be obtained from the equation

$$\sum_i f_i \frac{\varepsilon_i - \varepsilon}{\varepsilon_i + 2\varepsilon} = 0 \qquad (2)$$

The presence of water and ethanol as the solvent mixture was also investigated from the detailed transmittance spectra in the region 800–1300 nm, where the measured absorption bands at 975 and 1180 nm can be ascribed to water and to a combination of ethanol and water, respectively [13]. The latter band could also ascertain to unreacted alkoxide precusor, but an assumption that the matrix forming reaction is complete is made, as the matrix appears to be stable, and further evidence for the presence of ethanol and water was obtained from differential scanning calorimetry and thermogravimetric analysis.

The results obtained for each matrix are summarized in Table I. The characterization obtained for SiO_2 using this method is in agreement with previous work [13].

Table I. Composition of Titania and Silica Sol-Gel Matrices Obtained from Effective Media Theory [12][a]

Matix	Bulk oxide	Ethanol	Water	Void
Titania	47%	8%	15%	30%
Silica	56%	11%	18%	15%

[a] The values given are fractions per unit volume expressed as a percentage. A three-component model is chosen for both matrices.

According to these data significant differences between the two media can be found, namely, the higher porosity and structural order of TiO_2 compared to SiO_2. Moreover, the silica matrix is more efficient in retaining the solvents than the titania.

Reversible Protonation

We have examined the effect of pH on the absorption and fluorescence spectra (steady state and time resolved) of both porphyrins in ethanolic solution, since this is the solvent used in the synthesis of both matrices. Moreover, the matrix characterization (Table I) has shown that a significant amount of solvent persists in both matrices even after long stages of drying. The absorption and steady-state emission spectra of HTSPP ($\sim 10^{-6}\,M$) and ZnTSPP ($\sim 10^{-6}\,M$) in ethanol at different pH levels (by the addition of HCl or ammonia solution) are shown in Figs. 2 and 3, respectively.

The addition of ammonia to the HTSPP solution (pH 11) causes no significant shifts in either B or Q bands, but the B band is somewhat reduced (Fig. 2). The intensity of the first Q band is also reduced, whereas the second Q band becomes more intense, while the third is unaffected. However, the addition of HCl (pH 3) has strong effects upon both the B and the Q bands. In the Soret region the B band displays a red shift (to 444 nm) and new bands appear at 362 and 490 nm. The spectrum in the Q region shows only one prominent band, at 661 nm. At pH 3 and in agreement with previous studies [14], we ascribe the B band at 444 nm to the N-protonated

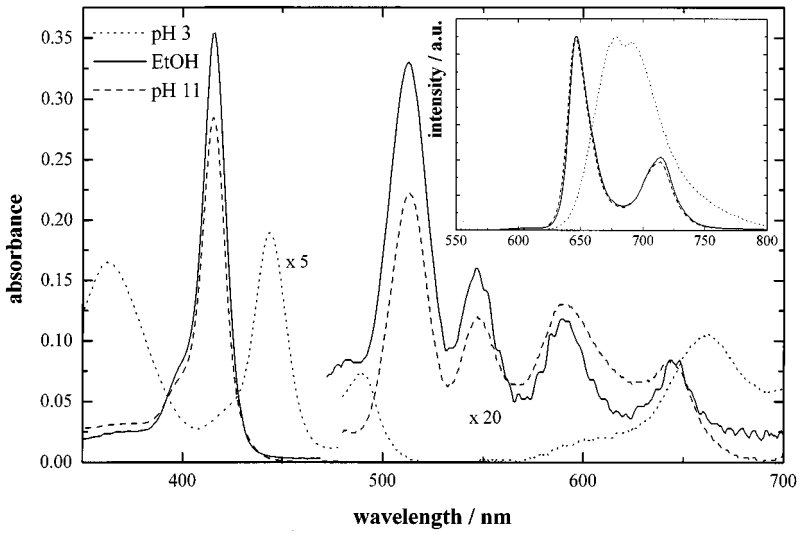

Fig. 2. Steady-state absorption and emission spectra for HTSPP in ethanol and at different pH levels (by addition of HCl and ammonia solution to ethanol).

species, H_4TSPP^{2-}, that is, the monomeric dianion, whereas the B band at 490 nm indicates the presence of aggregated porphyrin. It is well known that protonation of the porphyrin ring induces aggregation [15]. The increase in the D_{4h} symmetry of the molecule, upon the addition of two protons to the pyrrole units, promotes a simplification of the absorption spectrum [16], such as we have found.

The fluorescence emission spectra of the neutral and basic solutions, when excited at 418 nm, are shown in the inset in Fig. 2. The same emission is observed when either solution is excited in the respective Q bands. The acid solution was excited at 444 nm. An extremely weak emission could just be detected with excitation at 490 nm, thus confirming the low quantum yield of the aggregate emission [14]. In view of this, we assign the emission observed with excitation at 444 nm to the monomeric dianion.

The spectroscopic changes that ocurred upon the addition of HCl to the HTSPP solution could be reversed by the further addition of ammonia to the acidic ethanolic solution. The corresponding fluorescence lifetime mea-

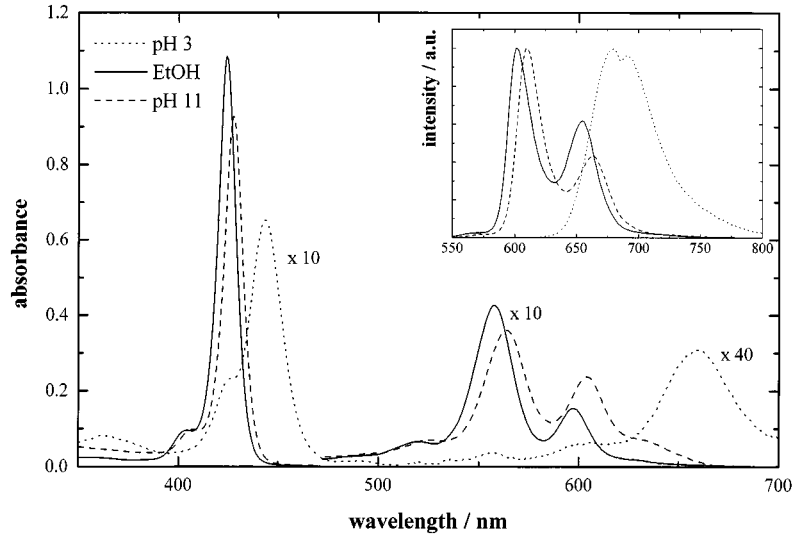

Fig. 3. Steady-state absorption and emission spectra for ZnTSPP in ethanol and at different pH levels (by addition of HCl and ammonia solution to ethanol).

surements are summarized in Table II. According to these data excitation in the B band at pH 11 and 7 produced emission with a predominant component, which we consider to be the lifetime of the free base. The recovered values were 10.6 ns in neutral ethanol and 12.1 ns in basic (pH 11) ethanol.

The decay measured for the acid solution has two components, 2.2 ns (60%) and 3.64 ns (34%). Since some aggregation can be detected in the absorption spectra, it is to be expected that the emission decay observed at this pH arises from the monomeric dianion with $\tau = 3.64$ ns and also from the aggregated dianion with $\tau = 2.24$ ns. This value is quite distinct from the value of 0.29 ns reported by Akins *et al.* [14] for the aggregate in acid aqueous solution in the presence of an electrolyte. Under their experimental conditions the 489-nm band displays the characteristically sharp features of closely coupled molecules forming a J-aggregate. Under our experimental conditions we believe that more labile aggregates can be formed, thus giving rise to a rather weak and broad 490-nm band and probably a new band at 362 nm.

Studies similar to those described above were performed with ZnTSPP under identical pH conditions. The results are shown in Fig. 3. The addition of ammonia causes a slight red shift in both the B and the Q bands. The same effect is observed in the correspondent emission spectra (see inset). At pH 3 the Soret band displays a maximum at 444 nm and a new band appears at 659 nm. The steady-state emission observed at this pH is identical to the emission of HTSPP at pH 3. In view of this we consider that, under acidic conditions, a significant demetallation of ZnTSPP has occurred and the emission observed is considered to originate from the dianion monomer, that is, from H_4TSPP^{2-}, although we cannot exclude the possibility of aggregation of protonated ZnTSPP.

Table II. Fluorescence Decay Times for HTSPP and ZnTSPP in Ethanol and Under Both Acidic (Addition of HCl) and Basic (Addition of Ammonia) Conditions[a]

Porphyrin	pH	λ_{exc} (nm)	τ_1 (ns)	I_1 (%)	τ_2 (ns)	I_2 (%)	χ^2
HTSPP	3	445	2.24 ± 0.18	66.1	3.64 ± 0.15	33.9	1.19
		416	2.50 ± 0.99	3.4	10.56 ± 0.05	96.6	1.17
	11	415	3.04 ± 1.86	1.6	12.13 ± 0.06	98.4	1.17
ZnTSPP	3	425	2.43 ± 0.18	78.2	4.17 ± 0.21	31.8	1.03
		425	2.09 ± 0.06	93.7	3.38 ± 0.57	6.3	1.12
	11	430	1.92 ± 0.12	96.0	7.97 ± 1.93	4.0	1.04

[a] The excitation was into the peak absorption and the emission was monitored at wavelengths >615 nm for HTSPP and >570 nm for ZnTSPP.

The measured lifetimes at pH 11 and in neutral ethanol show a dominant component ascribed to ZnTSPP in agreement with other authors [17]. On the other hand, the decay measured at pH 3 with excitation at 425 nm showed two components. The origin of these emissions cannot be unambigously identified under the experimental conditions used. Nevertheless, we consider that the predominant component with $\tau = 2.43$ ns probably originates from ZnTSPP in some degree of protonation, whereas the longer-lived component confirms the presence of pronated free-base porphyrin.

Spectroscopic Behavior on Incorporation in the Matrices

The absorption and fluorescence spectra of HTSPP incorporated in SiO_2 are shown in Fig. 4. In the Soret region the main absorption peak is broad and centered at 435 nm. A less intense peak was measured at 493 nm and minor peaks were also found in the Q region, the most intense of which occurs at 690 nm. The steady-state emission displays a maximum at 650 nm and a broad shoulder toward lower energies (~700 nm). Comparison of Figs. 2 and 4 shows that the porphyrin probes an acidic environment in the SiO_2 matrix. According to these data both the dianion monomer and an aggregate species are present.

The fluorescence decay analysis of this sample measured upon excitation at 435 nm is given in Table III. Two major components, 3.24 ns (46%) and 5.53 ns (50%), can be recovered, thus confirming the presence of the dianion monomer with a fluorescence lifetime of $\tau = 3.24$ ns [14]. The longer-lived component is considered to originate from some form(s) of an aggregate(s) of protonated porphyrin that is(are) likely to occur within the matrix pores. These can be considered as micro reaction vessels for the guest porphyrin, which we find also to contain solvent (Table I).

The effect of exposure to ammonia can be clearly detected from the recovered fluorescence decays of the porphyrin, which are shown, along with fitted functions and weighted residuals, in Fig. 5. In fact the dominant decay component is now the long-lived free base, H_2TSPP^{4-}, with $\tau = 10.6$ ns (88.3%); a minor component with $\tau = 2.8$ ns can be found, probably due to residual molecules of the dianion monomer, H_4TSPP^{2-}. The sample color changes reversibly from green (in acidic atmosphere) to purple (under ammonia vapour), an effect that can be easily observed with the naked eye.

The same porphyrin when incorporated in TiO_2 displays a somewhat different behavior as shown in Fig. 4. In fact the porphyrin is present as the free-base monomer

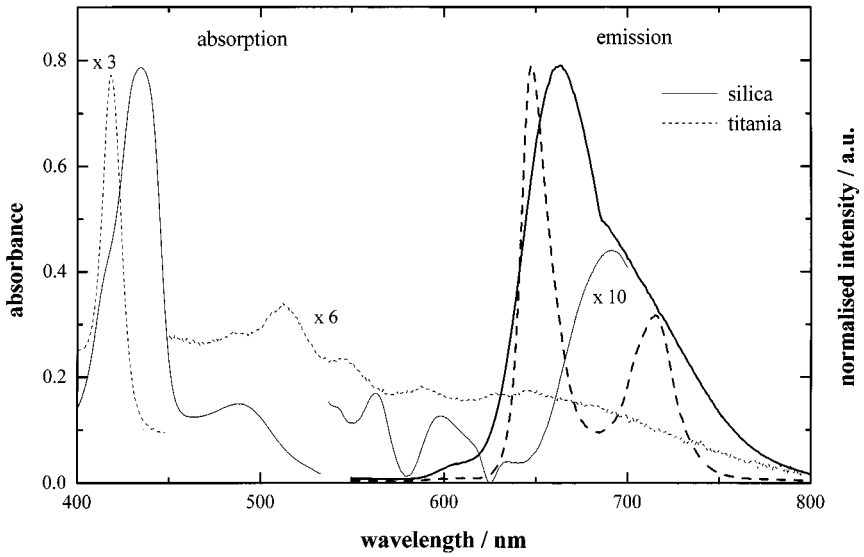

Fig. 4. Absorption and emission spectra for HTSPP in TiO_2 and SiO_2 sol-gel-derived matrices.

with the B band maximum at 419 nm. The steady-state emission of this sample correlates quite well with its absorption spectra, since the fluorescence spectrum displays the two well-known bands at 648 and 715 nm in a similar fashion to the neutral and basic ethanolic solutions. The recovered lifetimes shown in Table III confirm that the dominant form of HTSPP is the free base with a fluorescence lifetime of 10.8 ns (91%).

The effect of exposure to ammonia is therefore unimportant in this sample. This is confirmed by the decay measured after exposure to ammonia that reveals a major component with $\tau = 10.6$ ns (85.5%). These results can be understood in the light of the TiO_2 matrix characteristics. That is, a more porous and dry substrate where the guest molecule—the porphyrin—interacts mostly with the TiO_2 network. In this matrix the solvent is clearly less important than in the SiO_2 matrix, where the relative abundance of the solvent is definitely higher.

The behavior of ZnTSPP in TiO_2 is shown in Fig. 6. A profound decrease in the absorption of the sample during the drying process was found, thus confirming extensive decomposition of the ZnTSPP molecule. The emission spectrum shows the 600- and 650-nm bands of ZnTSPP and also a minor band at 715 nm, which is ascribed to the aggregate formed from the N-protonated TSPP (H_4TSPP^{2-}). This originates from extensive demetallation of the zinc porphyrin. The presence of the free base is further confirmed from the analysis of the decay of the ZnTSPP–SiO_2 sample by the presence of the long-lived component $\tau = 7.91$ ns (10.9%). Two fast compo-

Table III. Recovered Fluorescence Decay Values for Porphyrins in Both Types of Sol-Gel matrices, Both Before and After* Exposure to Ammonia

Matrix	λ_{exc} (nm)	τ_1 (ns)	I_1 (%)	τ_2 (ns)	I_2 (%)	τ_3 (ns)	I_3 (%)	χ^2
			(A) For HTSPP: Emission was monitored at wavelengths >615 nm					
Si	435	0.67 ± 0.60	3.9	3.24 ± 0.42	46.2	5.53 ± 0.12	49.9	1.06
Si*	415	0.42 ± 0.57	2.4	2.80 ± 0.54	9.3	10.57 ± 0.06	88.3	1.09
Ti	418			4.93 ± 0.90	9.1	10.81 ± 0.05	90.9	1.21
Ti*	418			6.89 ± 1.68	14.7	10.64 ± 0.12	85.3	1.16
			(B) For ZnTSPP: Emission was monitored at wavelengths >570 nm					
Si	420	1.62 ± 0.18	43.0	4.02 ± 0.34	41.8	9.88 ± 0.48	15.2	1.06
Si*	415	0.59 ± 0.30	4.3	3.38 ± 0.57	10.0	10.60 ± 0.07	85.7	1.06
Ti	427	0.42 ± 0.09	42.0	1.26 ± 0.06	47.1	7.91 ± 0.27	10.9	1.10
Ti*	427	0.56 ± 0.09	35.2	2.28 ± 0.27	19.0	10.09 ± 0.13	45.8	1.16

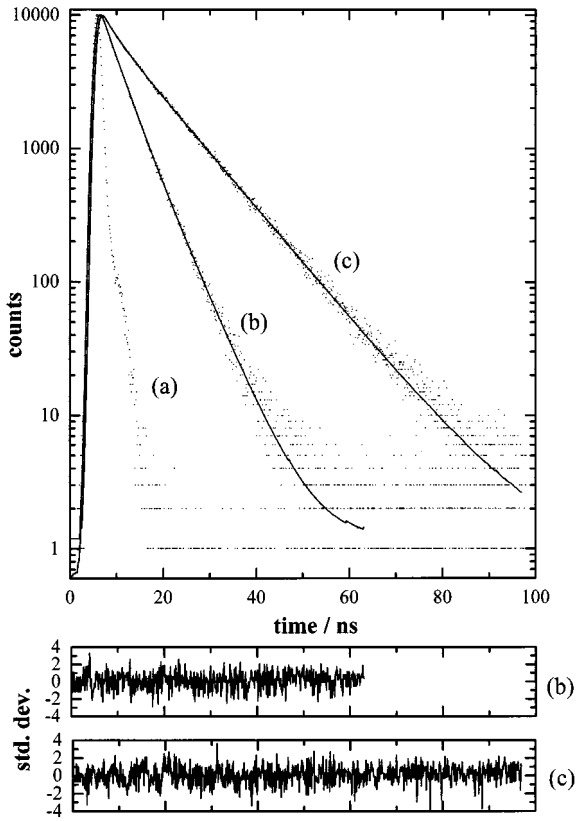

Fig. 5. The time-resolved fluorescence decay, fitted function, and weighted residuals for HTSPP in a SiO_2 matrix (b) before and (c) after exposure to ammonia vapor. The instrumental profile (a) is also shown.

nents, with lifetimes of 1.26 ns (47.1%) and 0.42 ns (42%), dominate this decay profile. We consider the assignment of these two components rather difficult in view of the demetallation process.

The absorption and emission spectra of ZnTSPP in SiO_2 are also shown in Fig. 6. The B band of the free base at 424 nm is very prominent and similar to what is observed in neutral or basic ethanol. The Q bands retain most of the features of ZnTSPP in neutral ethanol. In addition, a new band appears at 659 nm in a similar fashion to what was observed in acidic ethanol, where this new band was assigned to the dianion monomer. This feature is further confirmed by the steady-state emission spectrum, where the characteristic emission of H_4TSPP^{2-} at approximately 700 nm appears in the form of a shoulder in the usual ZnTSPP spectrum, with emission peaks at 600 and 650 nm. It is interesting to note that ZnTSPP when incorporated in SiO_2 becomes less prone to demetallation than in homogeneous acidic ethanol, as can be clearly seen by comparison of Figs. 6 and 3.

Finally, inspection of Table IIIB shows that the fluorescence decay can be resolved into three components, where τ_1 = 1.62 ns (43%) is ascribed to ZnTSPP and τ_2 = 4.0 ns (42%) and τ_3 = 9.9 ns (15.2%) to the dianion monomer and to the free base, respectively. Exposure to ammonia produces significant changes, in that now the long-lived component with τ = 10.6 ns (85.7%), attributed to the free base, is the dominant contribution to the decay. The steady-state fluorescence spectra (Fig. 7) also show that after exposure to ammonia, major similarities in spectrum shape are seen for both porphyrins. The

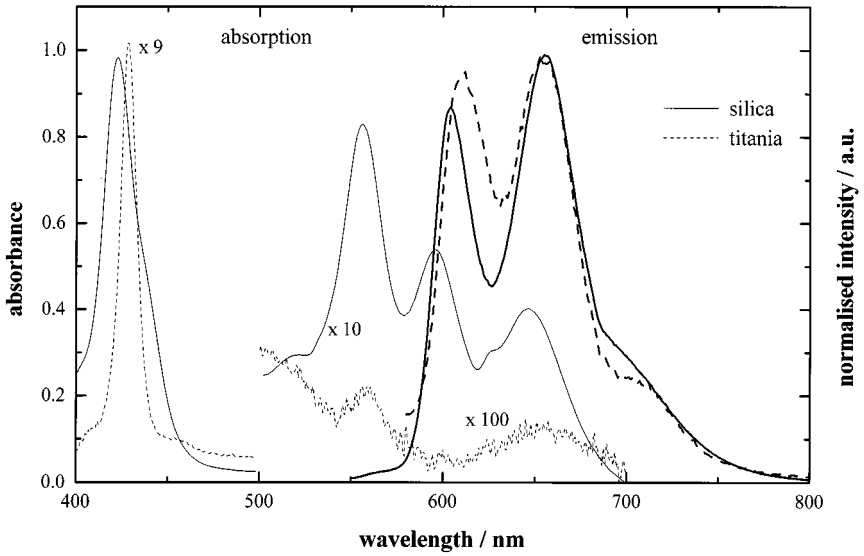

Fig. 6. Absorption and emission spectra for ZnTSPP in TiO_2 and SiO_2 sol-gel-derived matrices.

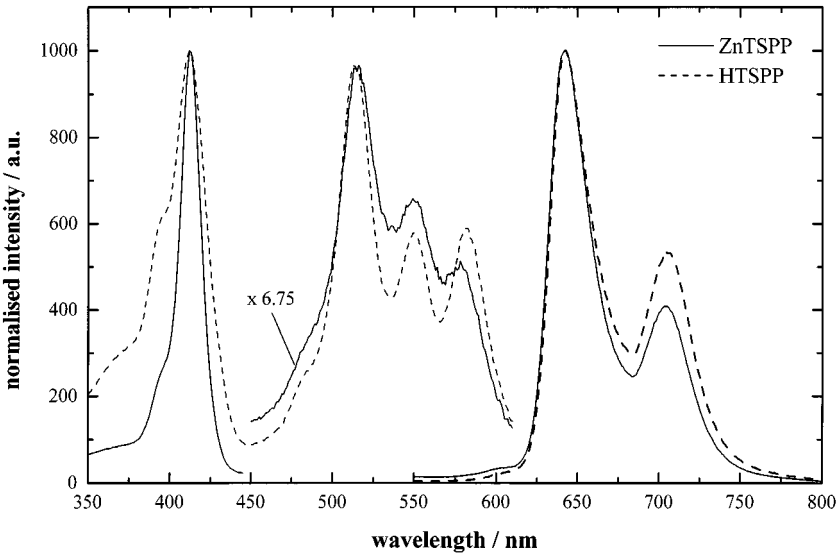

Fig. 7. Fluorescence excitation (monitored at 645 nm) and emission (with excitation at 415 nm) spectra for HTSPP and ZnTSPP incorporated into TEOS-derived matrices after exposure to ammmonia vapor for 5 h.

monomer band at about 600 nm for ZnTSPP is absent, which corroborates the time-resolved data in indicating the major demetallation of this porphyrin.

CONCLUSION

In this work we have shown that the spectroscopic behavior of the porphyrins is heavily influenced by their environment. HTSPP in the TEOS-derived matrix exists mainly in a protonated form, which can be readily converted to a free-base form by exposure to ammonia vapor. In the titania matrix, however, the free-base form is dominant from the outset and hence exposure to ammonia vapor produces little change in its spectroscopic characteristics. The major difference in the spectroscopic behavior of ZnTSPP when it is incorporated in the two types of matrix comes from the exposure to ammonia vapor. In the sol-gel-derived matrices there appears to be a greater degree of demetallation compared to basic ethanolic solution. For both porphyrins the effect of ammonia vapor is more pronounced with the silica matrix, which could lead to potential sensor applications. This could relate to the fact that this is a "wetter" matrix than the titania one and that the solvent retained in the pore structure plays an important role, while in the titania matrix the predominant interaction is that of the porphyrin with the bulk oxide.

ACKNOWLEDGMENTS

G.H. would like to thank the Fundação para a Ciência e a Tecnologia (PRAXIS XXI) for financial support.

REFERENCES

1. L. Emerson and E. Rabinowitch (1960) *Plant Physiol.* **35**, 477.
2. M. Gouterman (1959) *J. Chem. Phys.* **30**, 1139.
3. G. Hungerford, M. Van der Auweraer, J.-C. Chambron, V. Heitz, J.-P. Sauvage, J.-L. Pierre, and D. Zurita (1999) *Chem. Eur. J.* **5**, 2089–2100.
4. J. Zarzycky (1996) *J. Sol-Gel Sci. Technol.* **8**, 1–6.
5. K. Dou, X. Sun, X. Wang, and E. K. Knobe (1997) *SPIE Proc.* **3136**, 48–56. J.N. Demas and G.A Crosby (1971) *J. Non Cryst. Solids* **121**, 254–266.
6. R. Reisfeld (1990) *J. Non Cryst. Solids* **121**, 254–266.
7. D. Dolpphin (1978) *The Porphyrins, Vol. V,* Academic Press, New York, Chap. 7.
8. M. Ravikant, D. Reddy, and T. K. Chandrashekar (1991) *J. Chem. Soc. Dalton Trans.* 2103–2108.
9. This diffractogram was kindly made available to the authors by T. M. R. Viseu.
10. JCPDS—International Centre for Diffraction Data (1998) Search Manual, Files 38-448 and 21-1272.
11. J. I. Langford (1978) *J. Appl. Cryst.* **11**, 10–14.
12. I. Webman, J. Jortner, and M. H. Cohen (1977) *Phys. Rev. B* **15**, 5712–5723.
13. G. Hungerford, K. Suhling, and J. A. Ferreira (1999) *J. Photochem. Photobiol. A Chem.* **129**, 71–80.
14. D. L. Akins, S. Özçelik, H-R. Zhu, and C. Guo (1996) *J. Phys. Chem.* **100**, 14390–14396.
15. A. Harriman and M-C. Richoux (1984) *J. Photochem.* **27**, 205–214.
16. A. Stone and E. B. Fleisher (1968) *J. Am. Chem. Soc.* **90**, 2735.
17. M.-C. Richoux and A. Harriman (1982) *J. Chem. Soc. Faraday Trans. 1* **78**, 1873–1885.